Spectral domain optical coherence tomography imaging with an integrated optics spectrometer

V. Duc Nguyen,[1,*,†] B. Imran Akca,[2,4,†] Kerstin Wörhoff,[2] René M. de Ridder,[2] Markus Pollnau,[2] Ton G. van Leeuwen,[1,3] and Jeroen Kalkman[1]

[1]*Biomedical Engineering & Physics, Academic Medical Center, University of Amsterdam, Amsterdam, 1100 DE, Netherlands*

[2]*Integrated Optical MicroSystems Group, MESA + Institute for Nanotechnology, University of Twente, P.O. Box 217, 7500 AE, Enschede, Netherlands*

[3]*Biomedical Photonic Imaging, MIRA Institute for Biomedical Technology & Technical Medicine, University of Twente, P.O. Box 217, 7500 AE, Enschede, Netherlands*

[4]*e-mail: b.i.akca@ewi.utwente.nl*

**Corresponding author: d.v.nguyen@amc.uva.nl*

Received January 20, 2011; revised March 3, 2011; accepted March 10, 2011; posted March 10, 2011 (Doc. ID 141269); published March 31, 2011

We designed and fabricated an arrayed-waveguide grating (AWG) in silicon oxynitride as a spectrometer for spectral domain optical coherence tomography (SD-OCT). The AWG has a footprint of only 3.0 cm × 2.5 cm, operates at a center wavelength of 1300 nm, and has 78 nm free spectral range. OCT measurements are performed that demonstrate imaging up to a maximum depth of 1 mm with an axial resolution of 19 μm, both in agreement with the AWG design parameters. Using the AWG spectrometer combined with a fiber-based SD-OCT system, we demonstrate cross-sectional OCT imaging of a multilayered scattering phantom.

OCIS codes: 080.1238, 170.4500, 170.3880, 230.3120.

Optical coherence tomography (OCT) is an interferometric imaging technique that has developed rapidly over the last 20 years [1]. OCT has the ability to generate high-resolution cross-sectional images of biological tissue up to a few millimeters deep. Nowadays, OCT is used mainly in the clinic, particularly in ophthalmology. However, the use of OCT in medicine and other application areas is limited by its high cost and large instrument size. Integrated optics offers the potential to make OCT systems significantly smaller and more cost efficient [2–5].

In spectral domain OCT (SD-OCT), one of the most important components is the spectrometer in which light is dispersed via a diffraction grating onto a linescan camera. With the advent of integrated optics, miniature spectrometers have been developed based on two designs: grating-based spectrometers [6,7] and arrayed-waveguide grating (AWG) spectrometers [8]. In grating-based spectrometers, the locus of the focal points is an arc, whereas the linescan camera used for detection has a planar surface. The resulting defocus aberrations on the edges of the linescan camera lead to suboptimal imaging, which is a disadvantage for high-resolution imaging, as is required for OCT. In addition, grating-based spectrometers require deep-etching techniques that are complex, costly, and can suffer from optical losses induced by the nonverticality and roughness of the grating facets wavelength division. With the high spectral resolution and compactness, AWG spectrometers provide an excellent choice for SD-OCT. Recently, AWGs were used for ultrahigh-speed OCT imaging at 1.5 μm in SD-OCT through parallel signal acquisition using 256 balanced photoreceivers [9]. However, this system has the disadvantage that it uses optical amplifiers, is extremely costly, and has a high complexity.

In this study, we perform SD-OCT measurements at 1300 nm using a fiber-based interferometer, a simple linescan camera, and an imaging lens. The AWG spectrometers are designed in silicon oxynitride (SiON), which is transparent over a long wavelength range that covers all the frequently used OCT wavelength bands at 800, 1000, and 1300 nm. Good quality OCT images of a multilayered phantom are demonstrated.

The AWG structure includes input and output waveguides, free propagation regions (FPRs), an object plane, an image plane, and arrayed waveguides, as illustrated in Fig. 1. Light launched into the input waveguide diverges in the first FPR and is coupled into the arrayed waveguides. The length difference between adjacent waveguides in the array is an integer of the center wavelength. With this choice, the wavefront at the beginning of the second FPR is cylindrical and causes light of different wavelengths to be focused onto different locations in the image plane [8]. Finally, the dispersed light is coupled into different output waveguides.

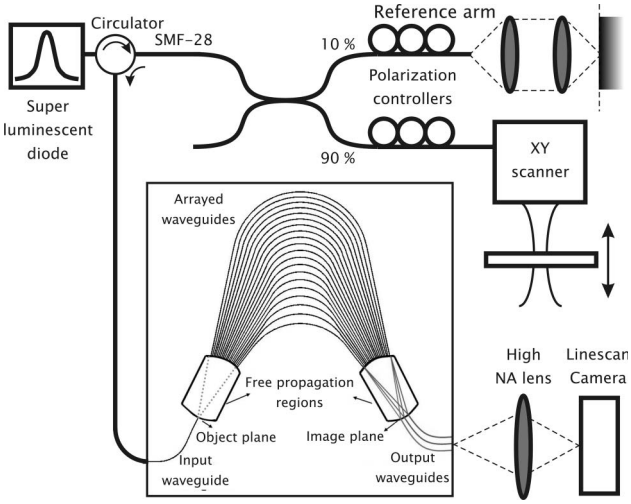

Fig. 1. Schematic of the experimental setup used for fiber-based SD-OCT with an AWG.

0146-9592/11/071293-03$15.00/0

For the AWG spectrometer used in this work, we aim at 18.5 μm depth resolution in air (calculated based on the transmission spectrum of the AWG spectrometer) and a maximum depth range in air of $z_{\max} = \lambda_c^2/(4n\delta\lambda) = 1$ mm, which is determined by the wavelength spacing $\delta\lambda$ between the output waveguides, the refractive index n of the medium, and the central wavelength $\lambda_c = 1300$ nm. These two requirements necessitate a large FSR of 78 nm and small wavelength spacing ($\delta\lambda = 0.4$ nm), which has been realized by choosing a diffraction order $m = 17$ and a path length difference of 15 μm between adjacent array waveguides. The AWG spectrometer consists of single-mode SiON channel waveguides of 2 μm width and 0.8 μm height. The upper cladding is a 4-μm-thick layer of silicon dioxide. The core and cladding refractive indices at 1.3 μm are 1.535 and 1.448, respectively. The minimum bending radius of curved waveguides is 500 μm. The minimum spacing between the 650 arrayed waveguides and between the 195 output waveguides is optimized using beam propagation method simulations in order to reduce loss and cross talk. The spacing between two adjacent output waveguides in the AWG image plane is 8 μm with a waveguide width of 4 μm (filling fraction $\alpha = 0.5$), resulting in –20 dB adjacent channel cross talk. The spacing of the waveguides at the output of the chip is 60 μm. The footprint of the AWG is only 3.0 cm × 2.5 cm.

A schematic of the fiber-based SD-OCT system with AWG spectrometer is shown in Fig. 1. Light from a broadband source (B&W Tek superluminescent diode, $\lambda_c = 1300$ nm, 40 nm FWHM, 7 mW output power) is coupled, via an optical circulator (Gould Fiber Optics), into a 90/10 beam splitter with polarization controllers positioned in both the sample and reference arms [10]. The backreflected light is redirected through the optical circulator and coupled into the input waveguide of the AWG spectrometer. The beams from the output waveguides of the AWG spectrometer are focused by a high-NA camera lens (JML Optical, focal length: 50 mm) onto a 46 kHz linescan camera (Sensors Unlimited SU-LDH-1.7RT/LC). A moveable mirror is placed in the sample arm to measure the OCT signals in depth. The acquired spectra are processed by subtracting the reference arm spectrum, then compensating for dispersion, and finally resampling to k space. The obtained spectra are Fourier transformed to obtain the OCT signals. The reference spectrum, which is the transmission spectrum of the AWG spectrometer, is used to calculate the theoretical axial resolution based on a cosine transform [11].

Figure 2 shows the reference spectrum and the interference spectrum after reference subtraction measured at 100 μm depth, both measured with the AWG spectrometer in the fiber-based SD-OCT. The wavelength scale is based on the AWG design parameters (λ_c and $\delta\lambda$), which determines the maximum imaging depth according to $z_{\max} = \lambda_c^2/(4n\delta\lambda)$. Figure 3(a) demonstrates OCT imaging up to the designed maximum depth range of 1 mm. The physical movement of the sample arm mirror corresponds one to one with the calculated depth scale. The measured signal-to-noise ratio (SNR) is 75 dB at 100 μm depth. The OCT roll-off in depth is fitted with a model [12] that is modified to include the noncontinuous sampling in the AWG image plane ($\delta k = \alpha/\delta\lambda$ in the Sinc term;

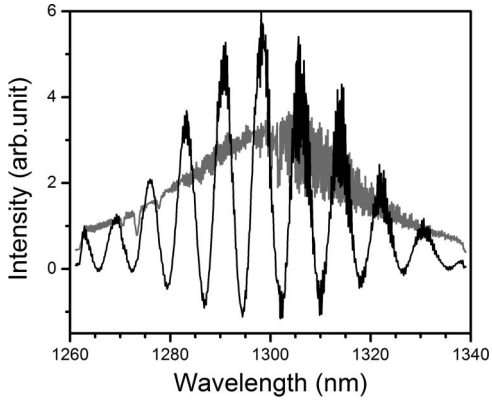

Fig. 2. Reference spectrum (gray curve) and interference spectrum (dark curve) after reference spectrum subtraction, both measured with the AWG spectrometer in the fiber-based SD-OCT.

dashed curve) [12]. The obtained ratio of the spectral resolution to the wavelength spacing ($\delta\lambda$) is $w = 1.7 \pm 0.1$, which is higher than the expected limit of the AWG performance, $w = 0.63$, calculated from the ratio of measured spectral resolution to the wavelength spacing. The theoretical axial resolution in air, calculated based on the reference spectrum, is 18.5 μm. Figure 3(b) shows the measured axial resolution, which is in reasonable agreement with the theoretical axial resolution. A slight decrease in depth resolution at larger depths and higher fitted w value is attributed to lens aberrations in the imaging system.

As a demonstration of OCT cross-sectional imaging using the AWG spectrometer, an image of a layered phantom is obtained by scanning the OCT beam over the sample (see Fig. 4). The phantom consists of three layers of scattering medium (scattering coefficient $\mu_s = 4\,\text{mm}^{-1}$,

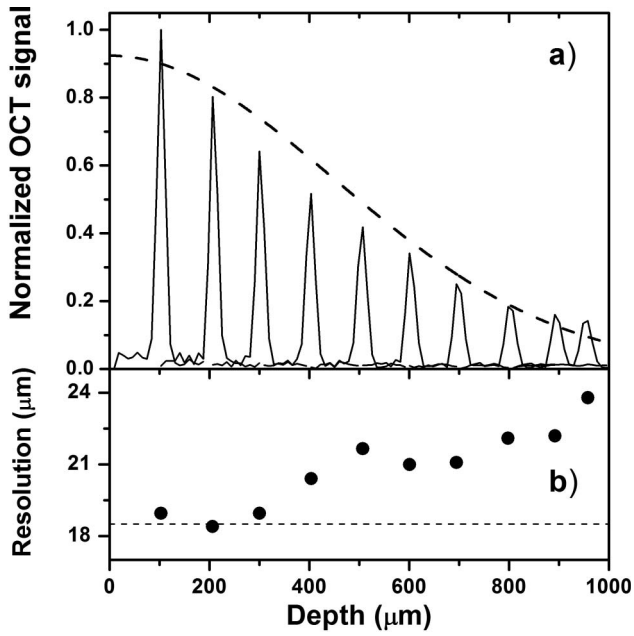

Fig. 3. (a) Measured OCT signal versus depth and fit of the roll-off (dashed curve). (b) Measured axial resolution (FWHM) versus depth in comparison with the theoretical axial resolution (dashed line). Both measurements are performed using the AWG in the fiber-based SD-OCT.

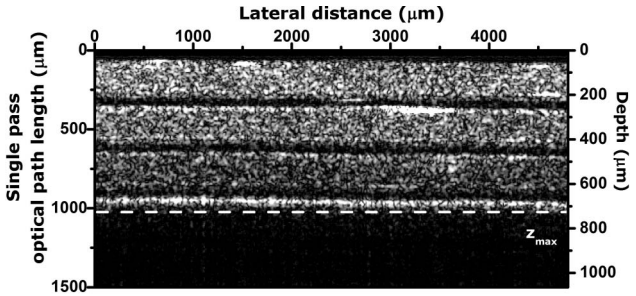

Fig. 4. OCT image of the three-layered scattering phantom measured with the AWG as spectrometer in SD-OCT. The dashed line indicates maximum imaging depth.

$n = 1.41$) [13] interleaved with nonscattering tape. As expected, all three scattering layers are observed up to the maximum single pass length of 1 mm (725 μm depth).

The current imaging resolution and depth are sufficient for biological imaging. Compared with bulk optics SD-OCT setups, our system has a lower SNR; however, the measured 75 dB OCT sensitivity includes 10 dB fiber-to-chip coupling loss [5], 4 dB AWG insertion loss, and chip-to-camera coupling losses. With improved fiber-to-chip coupling (e.g., using index-matching gel), we expect an SNR improvement of 10 dB. The spatial resolution and roll-off in depth match that of bulk optics OCT systems [12]. However, the depth range is smaller than bulk optics OCT system due to the limited number of output waveguides.

For a future reduction in AWG size and increase in the number of output channels, we propose to create a flat imaging plane in the second FPR [14] located on the edge of the chip. In that way, light can be imaged directly onto a linescan camera attached to the chip without the need for additional optics. In addition, by imaging a continuous spectrum directly onto the linescan camera, the sampling of the spectrum in k space is not limited by the number of output waveguides, but by the number of pixels on the camera, thereby facilitating a much larger maximum imaging depth.

In conclusion, we have demonstrated the use of a small-footprint SiON-based AWG spectrometer for SD-OCT. An imaging depth of 1 mm and an axial resolution of 19 μm in air are obtained. Finally, OCT imaging of a layered scattering phantom is demonstrated.

This work was supported by the Smart Mix Program of the Netherlands Ministry of Economic Affairs and the Netherlands Ministry of Education, Culture and Science.

[†]Contributed equally to the work and therefore should be considered equivalent authors.

References

1. D. Huang, E. A. Swanson, C. P. Lin, J. S. Schuman, W. G. Stinson, W. Chang, M. R. Hee, T. Flotte, K. Gregory, C. A. Puliafito, and J. G. Fujimoto, Science **254**, 1178 (1991).
2. D. Culemann, A. Knuettel, and E. Voges, IEEE J. Sel. Top. Quantum Electron. **6**, 730 (2000).
3. E. Margallo-Balbas, M. Geljon, G. Pandraud, and P. J. French, Opt. Lett. **35**, 4027 (2010).
4. G. Yurtsever, P. Dumon, W. Bogaerts, and R. Baets, Proc. SPIE **7554**, 75541B (2010).
5. V. D. Nguyen, N. Ismail, F. Sun, K. Wörhoff, T. G. van Leeuwen, and J. Kalkman, J. Lightwave Technol. **28**, 2836 (2010).
6. K. Chaganti, I. Salakhutdinov, I. Avrutsky, and G. W. Auner, Opt. Express **14**, 4064 (2006).
7. D. Sander and J. Müller, Sens. Actuators A Phys. **88**, 1 (2001).
8. M. K. Smit and C. van Dam, IEEE J. Sel. Top. Quantum Electron. **2**, 236 (1996).
9. D. Choi, H. Hiro-Oka, H. Furukawa, R. Yoshimura, M. Nakanishi, K. Shimizu, and K. Ohbayashi, Opt. Lett. **33**, 1318 (2008).
10. J. Kalkman, A. V. Bykov, D. J. Faber, and T. G. van Leeuwen, Opt. Express **18**, 3883 (2010).
11. A. Dubois, L. Vabre, A. C. Boccara, and E. Beaurepaire, Appl. Opt. **41**, 805 (2002).
12. N. A. Nassif, B. Cense, B. H. Park, M. C. Pierce, S. H. Yun, B. E. Bouma, G. J. Tearney, T. C. Chen, and J. F. de Boer, Opt. Express **12**, 367 (2004).
13. D. M. de Bruin, R. H. Bremmer, V. M. Kodach, R. de Kinkelder, J. van Marle, T. G. van Leeuwen, and D. J. Faber, J. Biomed. Opt. **15**, 025001 (2010).
14. S. Lu, C. Yang, Y. Yan, G. Jin, Z. Zhou, W. H. Wong, and E. Y. B. Pun, Opt. Express **13**, 9982 (2005).